explains why Hague and Kinley did not require hydrolyzed nickel(II) even at pH 8.

Unfortunately, the important question of the kinetic importance of intramolecular hydrogen bonding in salicylate anions remains unresolved. In the case that the monoanion of 3,5-dinitrosalicylate has normal reactivity, one is left with the difficulty of accounting for the low reactivity of the dianion. If the dianion has normal reactivity, then first bond formation and dissociation and subsequently chelate ring closing may be affected by hydrogen bonding in a way to account for the results. However, these are not overwhelming arguments for the kinetic effects of intramolecular hydrogen bonding.

Experimental Section

Materials. Salicylic acid (Matheson Coleman and Bell), 5-chlorosalicylic acid (Eastman), and 3,5-dinitrosalicylic acid (Matheson Coleman and Bell) were recrystallized from water before use. Aqueous nickel(II) perchlorate was prepared from nickel carbonate and standardized as described previously.[10] The buffer Pipes (1,4-piperazinebis(2-ethanesulfonic acid)) (Aldrich) was used as supplied. Solutions for kinetic studies were prepared in doubly distilled deionized water.

Kinetic Measurements. A 10-fold or greater molar excess of nickel(II) over ligand was used to ensure pseudo-first-order conditions. The two solutions of nickel(II) plus buffer (1.0×10^{-2} M) plus sodium perchlorate and ligand plus buffer (1.0×10^{-2} M) plus sodium perchlorate were adjusted to the desired pH and ionic strength (0.30 M) before mixing in the stopped-flow system. The recorded pH is that of the mixed solutions collected from the stopped-flow system. The pH before and after mixing generally differed by less than 0.04 unit. In one set of runs with salicylate the buffer concentration was changed to 5×10^{-3} M without detectable effect on the observed rate over the full pH range of the study.

The pH was measured on a Beckman Expandomatic meter using a 2.00 pH unit full-scale expansion. The meter was calibrated against standard buffers before use.

The optimum wavelengths for observation were determined from preliminary experiments on a Cary 219 spectrophotometer. The wavelengths used were 350, 340, and 360 nm for the salicylate, 5-chlorosalicylate, and 3,5-dinitrosalicylate systems, respectively.

A standard Aminco-Morrow stopped-flow system was used.[10] The transmittance-time curves were stored on a Tracor NS-570 signal averager and then output to a dual-trace oscilloscope for comparison to a synthetic exponential decay curve of variable, known time constant.[21] The recorded rate constants are the average of 5-8 replicate determinations.

Acknowledgment. The authors wish to acknowledge the financial support of the Natural Sciences and Engineering Research Council of Canada.

(21) Pinnell, D.; Jordan, R. B. *Inorg. Chem.* **1979**, *18*, 3191.

Contribution from Institut für Anorganische, Analytische und Physikalische Chemie der Universität Bern, CH-3000 Bern 9, Switzerland, and Department of Chemistry, University of Virginia, Charlottesville, Virginia 22901

Electron-Transfer Transitions in Hexachloroferrate(III). Single-Crystal Absorption and MCD Spectra

KURT NEUENSCHWANDER, HANS U. GÜDEL,* JOHN C. COLLINGWOOD, and PAUL N. SCHATZ*

Received July 14, 1982

Crystals of Cs_2NaYCl_6 doped with $FeCl_6^{3-}$ in which Fe^{3+} occupies sites of exact O_h symmetry were prepared by the Bridgman technique. Absorption and magnetic circular dichroism (MCD) spectra of $FeCl_6^{3-}$ were measured at low temperatures over the region 20000-45000 cm^{-1}. The observed features were attributed to ligand-to-metal electron-transfer transitions. The MCD spectrum is dominated by $\mathcal{C}$ terms which arise as a joint consequence of the ground-state spin degeneracy and the excited-state spin-orbit splittings. With use of a simple model, spin-orbit coupling effects are treated in detail, and a theoretical simulation of the MCD spectrum is presented that is in semiquantitative agreement with experiment. The energy ordering of the ligand donor orbitals is found to be $t_{1g} > t_{1u}(\pi + \sigma) > t_{2u} > t_{1u}(\sigma + \pi)$, and a best fit of the spectrum yields the spin-orbit coupling parameters $\zeta_{Fe} = 320$ cm^{-1} and $\zeta_{Cl} = 580$ cm^{-1} with about 10% σ-π mixing in the t_{1u} ligand orbitals.

Introduction

Hexachloro and hexabromo complexes of trivalent 3d transition-metal ions have received very little spectroscopic attention. This is in strong contrast to the corresponding octahedral complexes of rhenium(IV), iridium(IV), ruthenium(IV), molybdenum(IV), and osmium(IV), which have been thoroughly investigated by low-temperature single-crystal absorption and magnetic circular dichroism (MCD) spectroscopy.[1-8] The members of the first transition-metal series are chemically unstable in solution and can best be prepared from the melt. The cubic materials Cs_2NaYCl_6 and $Cs_2NaInCl_6$ served as host lattices for studies of the absorption, MCD (d-d transitions), and luminescence properties of $CrCl_6^{3-}$.[9,10] No other reports of absorption spectra of octahedral MX_6^{3-} (M = 3d metal; X = Cl, Br) are found in the literature. A diffuse powder reflectance spectrum of $(NH_4)_4 \cdot FeCl_6 \cdot SbCl_6$ in the region of the d-d transitions has been reported.[11]

Ligand-to-metal charge-transfer (CT or electron transfer) transitions were of primary interest in the studies of MX_6^{n-} complexes of the second and third transition-metal series. The relative order of donor ligand orbitals was unambiguously established on the basis of the MCD results.[1,3-8] Electron-transfer transitions were also investigated in tetrahedral

* To whom correspondence should be addressed: H.U.G., Universität Bern; P.N.S., University of Virginia.

(1) Henning, G. N.; McCaffery, A. J.; Schatz, P. N.; Stephens, P. J. *J. Chem. Phys.* **1968**, *48*, 5656.
(2) Jørgensen, C. K. *Prog. Inorg. Chem.* **1970**, *12*, 101.
(3) Piepho, S. B.; Lester, T. E.; McCaffery, A. J.; Dickinson, J. R.; Schatz, P. N. *Mol. Phys.* **1970**, *19*, 781.
(4) Bird, B. D.; Day, P.; Grant, E. A. *J. Chem. Soc. A* **1970**, 100.
(5) Piepho, S. B.; Dickinson, J. R.; Spencer, J. A.; Schatz, P. N. *Mol. Phys.* **1972**, *24*, 609.
(6) Collingwood, J. C.; Schwartz, R. W.; Schatz, P. N.; Patterson, H. H. *Mol. Phys.* **1974**, *27*, 1291.
(7) Collingwood, J. C.; Piepho, S. B.; Schwartz, R. W.; Dobosh, P. A.; Dickinson, J. R.; Schatz, P. N. *Mol. Phys.* **1975**, *29*, 793.
(8) Collingwood, J. C.; Schatz, P. N.; McCarthy, P. J. *Mol. Phys.* **1975**, *30*, 469.
(9) Schwartz, R. W. *Inorg. Chem.* **1976**, *15*, 2817.
(10) Güdel, H. U.; Snellgrove, T. R. *Inorg. Chem.* **1978**, *17*, 1617.
(11) Yamatera, H.; Kato, A. *Bull. Chem. Soc. Jpn.* **1968**, *41*, 2220.

0020-1669/83/1322-1712$01.50/0 © 1983 American Chemical Society

$FeCl_4^-$,[12] in octahedral $FeCl_5(H_2O)^{2-}$,[13] and in the low-spin complex $Fe(CN)_6^{3-}$.[14] An MCD study of tris(acetylacetonato)iron(III) in solution and polymer films has also been reported by Vliek and Zandstra.[15] These authors do not propose detailed spectral assignments but suggest that their observed MCD temperature dependence is chiefly due to spin–orbit mixing of excited states with the $^6A_1$ ground state. In contrast we shall interpret our results exclusively on the basis of spin–orbit effects in electronic excited states.

On the basis of Jørgensen's concept of optical electronegativity, a large number of Cl → Fe electron-transfer transitions are expected between 20000 and 50000 cm^{-1} in $FeCl_6^{3-}$.[2] This complex, therfore, should serve as a good prototype for MX_6^{3-} complexes of the 3d series. We therefore prepared crystals of Cs_2NaYCl_6 doped with appropriate amounts of $FeCl_6^{3-}$ and investigated their spectroscopic properties in the near-UV region. Cs_2NaYCl_6 was chosen as a host because of its transparency up to ~45000 cm^{-1} and the fact that it does not undergo a phase transition between room and liquid-helium temperature.[9,16]

Experimental Section

A. Preparations. The following starting materials were used: CsCl (p.A., Merck), NaCl (p.A., Merck), YCl_3 anhydrous (ROC/RIC), and $FeCl_3$ anhydrous (zur Synthese, Merck). $FeCl_3$ was twice sublimed before use. A stoichiometric mixture of CsCl (2 parts), NaCl (1 part), and YCl_3 (1 part) was finely powdered in a drybox, poured into a dry silica ampule, dried at 400 °C for 3 h, and melted under vacuum. After the mixture cooled, 0.1 mol % of $FeCl_3$ was added in the drybox. The ampule was then evacuated and closed. Crystals were grown by the Bridgman technique. In our apparatus, which was built in Bern, the ampule was stationary and the furnace, after melting the mixture at 850 °C, was raised at a rate of 0.03 mm/min.

Light yellow transparent boules were obtained. There was a concentration gradient in the crystals, with the iron content highest in the upper part of the boule. The samples were analyzed for Fe by standard techniques. The crystals are moderately hygroscopic.

B. Spectra. Cleavage planes of the crystals were identified by X-ray back-scattering as {001}. They were polished and used for all the absorption and MCD experiments. The magnetic field, therefore, was always along one of the fourfold axes of the $FeCl_6^{3-}$ complexes.

Absorption spectra were measured on a Cary 17 spectrometer equipped with an EMI 9783 R photomultiplier for increased sensitivity in the near-UV region.

The principle and experimental setup used for the MCD measurements has recently been described.[17] An Oxford Instruments Spectromag IV cryomagnet providing temperatures down to 1.4 K and magnetic fields up to 5 T was used. Depolarization by the crystal was found to be negligible at 500 nm. Beyond about 38000 cm^{-1} the MCD has only qualitative significance. The signal-to-noise ratio in this region becomes increasingly unfavorable because of the sharply rising absorption edge of the crystal host and the decreasing intensity of the light source.

Theory

A. General Considerations. The site symmetry of Y in Cs_2NaYCl_6 is O_h. From analogy to lanthanide-doped Cs_2NaYCl_6 systems, which have been studied by ESR,[16] we can assume that Fe substitutes for Y in the doped crystals and thus resides at sites of exactly octahedral symmetry.

Formally allowed electronic transitions in $FeCl_6^{3-}$ are either electron-transfer transitions from weakly bonding or nonbonding ligand donor orbitals to the partly filled 3d orbitals of the metal or intraatomic transitions like 3d → 4s, 4p on the iron atom. The latter transitions are expected to lie well above 50000 cm^{-1}. The moderately intense absorptions between 24000 and 45000 cm^{-1} are therefore Cl → Fe CT transitions. Their relatively low intensity compared to that of the corresponding transitions in 4d and 5d MX_6^{n-} complexes may be due to the lower covalency of the M–Cl bonds.

Table I. LS States ($\Gamma_4 S_4$) of $FeCl_6^{3-}$ Produced from Fe^{2+} Quintet States ($\Gamma_3 S_3$)

x^a	n	S_1	$\Gamma_1{}^b$	S_2	$\Gamma_2{}^c$	S_3	Γ_3	S_4	Γ_4
1	1	1	T_{1g}	1	A_{2g}	2	T_{2g}	3/2, 5/2	A_{2u}, E_u, T_{1u}, T_{2u}
1	0	3/2	A_{2g}	1/2	E_g	2	E_g	3/2, 5/2	T_{1u}, T_{2u}
2	1	1	T_{1g}	1	A_{2g}	2	T_{2g}	3/2, 5/2	A_{1u}, E_u, T_{1u}, T_{2u}
2	0	3/2	A_{2g}	1/2	E_g	2	E_g	3/2, 5/2	T_{1u}, T_{2u}

[a] Ligand orbital t_{xu}. [b] From configuration t_{2g}^{3+n}. [c] From configuration e_g^{3-n}.

B. Spin–Orbit Coupling. The $^6A_{1g}$ electronic ground state of $FeCl_6^{3-}$ derives from the high-spin $t_{2g}^3 e_g^2$ d-electron configuration. Zero-field splittings due to second-order mixing with excited states are on the order of 10^{-2}–10^{-3} cm^{-1} and can be neglected. At 4.2 K the magnetic anisotropy is negligibly small and $g \approx 2.0$.[18] Thus we treat the ground state of the system throughout as $^6A_{1g}$ unsplit by any perturbations.

The ligand-to-metal CT states of interest all arise from the three open-shell configurations $t_{xu}{}^5 t_{2g}{}^{3+n} e_g{}^{3-n}$ ($n = 0, 1$; $x = 1, 2$), where t_{xu} may be the ligand MO $t_{1u}(\sigma + \pi)$, $t_{2u}(\pi)$, or $t_{1u}(\pi + \sigma)$.[1-8] Electric-dipole-allowed transitions are $^6A_{1g} \rightarrow {}^6T_{1u}$, and each excited configuration gives rise to one $^6T_{1u}$ state. These $^6T_{1u}$ states are split by first-order spin–orbit coupling *and* can spin–orbit mix with many of the other CT states (as well as with each other). Thus we may anticipate a wide dispersion of the allowed intensity within the excited-state manifolds.

In the absence of detailed knowledge of the electrostatic interactions in the excited configurations, we make the following simplifying assumptions.

(1) Electrostatic interaction between electrons in the ligand (t_{1u}, t_{2u}) and metal molecular orbitals (t_{2g}, e_g) are negligible.

(2) The ligand field states arising from the $t_{2g}{}^{3+n} e_g{}^{3-n}$ configurations are those calculated for octahedral Fe^{2+}.

(3) Both in-state (within a given $^6T_{1u}$) and out-of-state spin–orbit effects must be treated. In the latter case, however, spin–orbit mixing is considered only between each $^6T_{1u}$ state and those states that, because of our model, are (accidentally) degenerate with it (see later). We refer to the in-state case as the "simple" (first-order) treatment; inclusion of the degenerate out-of-state mixing contributions constitutes the "full" (first-order) treatment.

Our model thus views the excited states as arising from $[Fe^{2+},(Cl_6)^{5-}]^{3-}$ with no interactions between electrons in the Fe^{2+} molecular orbitals with those in the $(Cl_6)^{5-}$ molecular orbitals. This type of model has been surprisingly successful in treating the second and third transition series hexahalides,[6-8] and in any event, unless a detailed quantum-mechanical calculation of the excited eigenstates is attempted, neglect of ligand–metal interactions is essential if the treatment of spin–orbit coupling is to be tractable.

Consistent with the model, we adopt the coupling scheme

$$\{t_{xu}{}^5(^2T_{xu}),\ [(t_{2g}{}^{3+n}(^{2S_1+1}\Gamma_1),\ e_g{}^{3-n}(^{2S_2+1}\Gamma_2))^{2S_3+1}\Gamma_3]\}^{2S_4+1}\Gamma_4$$

This nomenclature means the following: the (LS) state $^{2S_1+1}\Gamma_1$ from the Fe^{2+} configuration $t_{2g}{}^{3+n}$ is coupled to the state $^{2S_2+1}\Gamma_2$ from the Fe^{2+} configuration $e_g{}^{3-n}$ to produce the Fe^{2+} state $^{2S_3+1}\Gamma_3$, which in turn is coupled to the state $^2T_{xu}$ from the

(12) Rivoal, J. C.; Briat, B. *Mol. Phys.* **1974**, *27*, 1081.
(13) Kambli, U.; Güdel, H. U. *Inorg. Chem.* **1982**, *21*, 1270.
(14) Schatz, P. N.; McCaffery, A. J.; Suëtaka, W.; Henning, G. N.; Ritchie, A. B.; Stephens, P. J. *J. Chem. Phys.* **1966**, *45*, 722. Stephens, P. J. *Inorg. Chem.* **1965**, *4*, 1690.
(15) Vliek, R. M. E.; Zandstra, P. J. *Mol. Phys.* **1976**, *32*, 151.
(16) Schwartz, R. W.; Watkins, S. F.; O'Connor, C. J.; Carlin, R. L. *J. Chem. Soc., Faraday Trans. 2* **1976**, *72*, 565.
(17) Geiser, U.; Güdel, H. U. *Inorg. Chem.* **1981**, *20*, 3013.
(18) Bill, H.; Neuenschwander, K., unpublished results.

ligand configuration t_{xu}^5 to produce the required state $^{2S_4+1}\Gamma_4$ of $FeCl_6^{3-}$ ($t_{xu}^5 t_{2g}^{3+n} e_g^{3-n}$).

Since the ligand states are doublets, $^6T_{1u}$ states of $FeCl_6^{3-}$ can be produced only from quintet states of Fe^{2+}. There are just two such states, namely, $^5T_{2g}$ from $t_{2g}^4(^3T_{1g})$, $e_g^2(^3A_{2g})$ and ^5E_g from $t_{2g}^3(^4A_{2g})$, $e_g^3(^2E_g)$, the latter being $10Dq$ higher in energy. The complete set of $FeCl_6^{3-}$ LS states produced by coupling these quintets with the ligand doublets is listed in Table I. Note particularly that, by assumption 1 of our model (see above), *all the quartet and sextet states for a specified value of x and n are (accidentally) degenerate.* Thus, for example, for $x = 1$, $n = 1$, the *degenerate* set of LS states is (Table I) $^4A_{2u}$, $^6A_{2u}$, ^4E_u, ^6E_u, $^4T_{1u}$, $^6T_{1u}$, $^4T_{2u}$, $^6T_{2u}$. In this case, for example, the simple treatment requires diagonalization of the spin–orbit coupling operator only within the $^6T_{1u}$ manifold; the full treatment requires a diagonalization using as the basis the eight (degenerate) LS states just listed.

Many other $FeCl_6^{3-}$ LS states can be formed by coupling the ligand doublets with the Fe^{2+} triplets and singlets. However, *none of these* should be degenerate with a $^6T_{1u}$ state and by assumption 3 of the model (see above), all such states are ignored.

The heart of the spin–orbit coupling calculation is thus the evaluation of matrix elements of the form

$$\langle ^{4,6}\Gamma_4|\hat{\mathcal{H}}_{so}|^{4,6}\Gamma_4'\rangle \quad (1)$$

where $\hat{\mathcal{H}}_{so} = \sum_i \xi_i(r_i)\mathbf{l}_i\cdot\mathbf{s}_i$ is the spin–orbit coupling operator and Γ_4 and Γ_4' both arise from coupling the same ligand state with the same Fe^{2+} state (i.e., Γ_4 and Γ_4' are in the same row and last column of Table I). Evaluation of these matrix elements is complicated because the LS states involved have three open shells, and recourse to the irreducible tensor method is essential. There are now two versions of this technique available: the older method of Griffith[19] (with corrections by Silver[20]) and the chain of groups approach of Butler.[21] For evaluation of the spin–orbit matrix elements of interest here, the Butler approach is probably an order of magnitude faster. The Griffith approach requires a tedious series of couplings and uncouplings to relate eq 1 to the corresponding many-electron reduced matrix elements.[19] The Butler approach entirely avoids this process by using the Racah factorization lemma.[21] It is thus possible[22] to write the desired result in terms of phase factors and a few symmetry-determined coefficients, *all of which are available in tables.* As a consequence, this method is not only very much faster but is also much less prone to error. This application of the Butler approach to the calculation of spin–orbit matrix elements is due to Dr. S. B. Piepho. In the Appendix, we describe this method briefly with an example and contrast it with the older Griffith approach. In the present work, all spin–orbit matrices were calculated by both methods. The resulting eigenvalues agreed in all cases.

C. Theoretical MCD Spectrum. The theoretical MCD dispersion may be written[23]

$$\frac{\Delta A}{\mathcal{E}} = 152.5\sum_i \left[-\mathcal{A}_1^{(i)}\frac{\partial f_i(\mathcal{E})}{\partial \mathcal{E}} + (\mathcal{B}_0^{(i)} + \mathcal{C}_0^{(i)}/kT) f_i(\mathcal{E}) \right] cl \quad (2)$$

and the corresponding zero-field absorption spectrum is given by

$$\frac{A^0}{\mathcal{E}} = 326.6\sum_i \mathcal{D}_0^{(i)} f_i(\mathcal{E}) cl \quad (3)$$

where the sum is over all transitions, ΔA (the MCD per Tesla) $= A_L - A_R$, with A_L and A_R being the absorbances (optical densities) for left and right circularly polarized light in the presence of the field, kT is in cm^{-1}, A^0 is the zero-field absorbance, $\mathcal{E}$ is the photon energy (in cm^{-1}), c is the sample concentration, and l is its thickness. $f_i(\mathcal{E})$ is the absorption line shape of the ith transition, and $\mathcal{A}_1^{(i)}$, $\mathcal{B}_0^{(i)}$, and $\mathcal{C}_0^{(i)}$ determine the contributions of the $\mathcal{A}$, $\mathcal{B}$, and $\mathcal{C}$ terms, respectively, to the MCD; $\mathcal{D}_0^{(i)}$ is the corresponding dipole strength. Equation 2 assumes that Zeeman splittings are small compared to band widths and kT and that the rigid shift model[23] is applicable.

The ground state of our system is $^6A_{1g}$ with $g \approx 2.0$, and there is significant spin–orbit mixing in the excited states. We therefore anticipate strong $\mathcal{C}$ terms in the MCD. (These terms have an absorption-like shape, vary as $1/T$, and are a consequence of population differentials among the Zeeman split sublevels of the ground state.[23,24]) Furthermore, since the bands are broad, $\mathcal{A}$-term contributions to the MCD dispersion are expected to be small relative to the $\mathcal{C}$ terms, especially at low temperature. (The $\mathcal{A}$ term is temperature independent, has a derivative (of the absorption) lineshape, and is a consequence of Zeeman shifts in the ground and/or excited state. The peak to trough of the $\mathcal{A}$ term various inversely with the second power of the line width.[23,24]) Finally, $\mathcal{B}$ terms are possible due to magnetic-field-induced mixing of zero-field states,[23,24] particularly as a result of field-induced mixing among excited-state spin–orbit components. ($\mathcal{B}$ terms are also temperature independent and have an absorption-like line shape.[23,24]) It is an experimental fact, however, that the MCD is completely dominated by $\mathcal{C}$ terms (see Results). We therefore need only calculate the $\mathcal{C}$-term contribution to the MCD dispersion, and thus we set $\mathcal{A}_1^{(i)} = \mathcal{B}_0^{(i)} = 0$ in eq 2 for all i.

For transition $A \rightarrow J$ we use the expressions[22,23]

$$\mathcal{C}_0(A \rightarrow J) = \frac{-1}{|A|}\sum_{\alpha\lambda}\langle A\alpha|L_Z + 2S_Z|A\alpha\rangle(|\langle A\alpha|m_{-1}|J\lambda\rangle|^2 - |\langle A\alpha|m_{+1}|J\lambda\rangle|^2) \quad (4)$$

$$\mathcal{D}_0(A \rightarrow J) = \frac{1}{2|A|}\sum_{\alpha\lambda}(|\langle A\alpha|m_{-1}|J\lambda\rangle|^2 + |\langle A\alpha|m_{+1}|J\lambda\rangle|^2) \quad (5)$$

where $|A|$ is the degeneracy of the ground state (6 in the present case), $m_{\pm 1} = \mp(1/2^{1/2})(m_x \pm im_y)$, $\mathbf{m}$ is the electric dipole operator, and $\mathbf{L}$ and $\mathbf{S}$ are the orbital and spin angular momentum operators. Only the ground-state functions need be diagonal in $L_Z + 2S_Z$. In our present application, the ground state is $|A\alpha\rangle = |^6A_{1g}M_s a_{1g}\rangle$. Each excited state $|J\lambda\rangle$ can be written as a linear combination of $|^6T_{1u}M_s\theta\rangle$ ($\theta = +1, 0, -1$) and all the degenerate quartet and sextet (LS) states that are coupled to it by the spin–orbit operator (the $|S_4\Gamma_4\rangle$ of Table I). However, only $\langle ^6A_{1g}M_s a_{1g}|m_{\pm 1}|^6T_{1u}M_s\theta\rangle \neq 0$, and thus to evaluate eq 4 and 5, it is only necessary to know the coefficient of $|^6T_{1u}M_s\theta\rangle$ in each $|J\lambda\rangle$. (In the simple treatment these coefficients are simple symmetry-determined factors.) These are obtained by transforming the $|J\lambda\rangle$ appropriately (see Appendix). Summations over M_s and θ are

(19) Griffith, J. S. "The Irreducible Tensor Method for Molecular Symmetry Groups"; Prentice-Hall: Englewood Cliffs, NJ, 1962.
(20) Silver, B. L. "Irreducible Tensor Methods"; Academic Press: New York, 1976.
(21) Butler, P. H. "Point Group Symmetry Applications"; Plenum Press: New York, 1981.
(22) Piepho, S. B.; Schatz, P. N. "Group Theory in Spectroscopy With Applications to Magnetic Circular Dichroism"; Wiley-Interscience: New York, 1983.
(23) Stephens, P. J. *Adv. Chem. Phys.* **1976**, *35*, 197.
(24) Schatz, P. N.; McCaffery, A. J. *Q. Rev., Chem. Soc.* **1969**, *23*, 552–584; **1970**, *24*, 329.

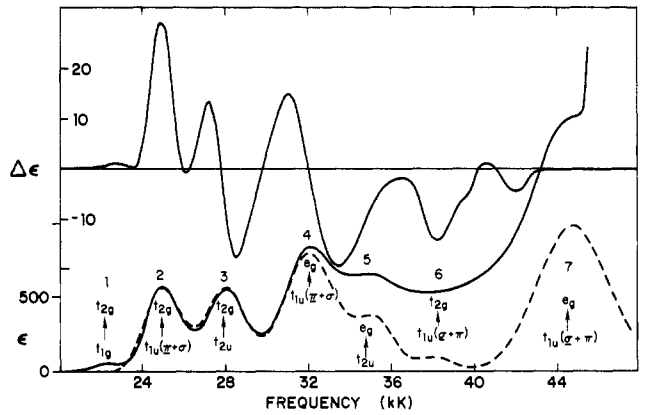

Figure 1. Experimental absorption spectrum at 8 K (ϵ = molar extinction coefficient) and MCD spectrum at 4.2 K ($\Delta\epsilon = \epsilon_L - \epsilon_R/T$) of $FeCl_6^{3-}$ doped into Cs_2NaYCl_6. The bands are numbered and assigned according to the discussion in the text. The dashed absorption spectrum is a Gaussian fit with the following parameters (eq 6 and 7): $\nu_0(2) = 24900$, $\Delta_2 = 1170$, $\mathcal{D}_0(2) = 0.1574$; $\nu_0(3) = 27900$, $\Delta_3 = 1320$, $\mathcal{D}_0(3) = 0.1527$; $\nu_0(4) = 32000$, $\Delta_4 = 1700$, $\mathcal{D}_0(4) = 0.2438$; $\nu_0(5) = 35200$, $\Delta_5 = 1250$, $\mathcal{D}_0(5) = 0.0700$; $\nu_0(6) = 38100$, $\Delta_6 = 1330$, $\mathcal{D}_0(6) = 0.0187$; $\nu_0(7) = 44800$, $\Delta_7 = 2500$, $\mathcal{D}_0(7) = 0.3000$. ν_0 and Δ are in cm^{-1}; $\mathcal{D}_0$ is in D^2.

Table II. Positions and Intensities of Absorption and MCD Band Maxima (Minima)

abs band	$\nu_{max,min}$, 10^3 cm^{-1}	ϵ_{max}	$\Delta\epsilon_{max}$/T(4.2 K)	transition
1	22.4	73	+2.4	$t_{1g} \rightarrow t_{2g}$
	24.6		+30.4	
2	24.9	619		$t_{1u}(\pi + \sigma) \rightarrow t_{2g}$
	25.8		−0.4	
	26.9		+14.6	
3	27.9	579		$t_{2u} \rightarrow t_{2g}$
	28.2		−18.0	
	30.7		+16.5	
4	32.0	845		$t_{1u}(\pi + \sigma) \rightarrow e_g$
	33.7		−18.4	
5	35.0	644[a]		$t_{2u} \rightarrow e_g$
6	38.1	496[a]	−13.3	$t_{1u}(\sigma + \pi) \rightarrow t_{2g}$
7	41.9		−3.7	
	44.8	1740[a]		$t_{1u}(\sigma + \pi) \rightarrow e_g$

[a] Note that these values are upper limits for $FeCl_6^{3-}$ because of the Cs_2NaYCl_6 host absorption edge which rises rapidly toward the blue end of the spectrum.

then performed to obtain each $\mathcal{C}_0^{(i)}$ and $\mathcal{D}_0^{(i)}$.

In our later simulations, the line shapes are represented by normalized Gaussians:

$$f_i(\nu) = \frac{1}{\Delta_i \pi^{1/2}} \exp\left(-\frac{(\nu - \nu_0(i))^2}{\Delta_i^2}\right) \quad (6)$$

With use of this expression in eq 3, the dipole strength ($\mathcal{D}_0$) is related to the experimental integrated intensity by

$$\mathcal{D}_0 = (1/326.6cl) \int \frac{A^0}{\mathcal{E}} \, d\mathcal{E} \quad (7)$$

Results

The experimental low-temperature absorption and MCD spectra of $Cs_2NaYCl_6:Fe^{3+}$ are shown in Figure 1 over the range 20000–45000 cm^{-1}. Band positions and intensities are collected in Table II. All the MCD bands show the same temperature dependence and the same saturation behavior. The lower panel of Figure 2 shows that at low temperature the MCD signal varies as $1/T$ with an intercept ~ 0. This demonstrates that $\mathcal{C}$ terms dominate and justifies our approximation, $\mathcal{A}_1^{(i)} = \mathcal{B}_0^{(i)} = 0$.

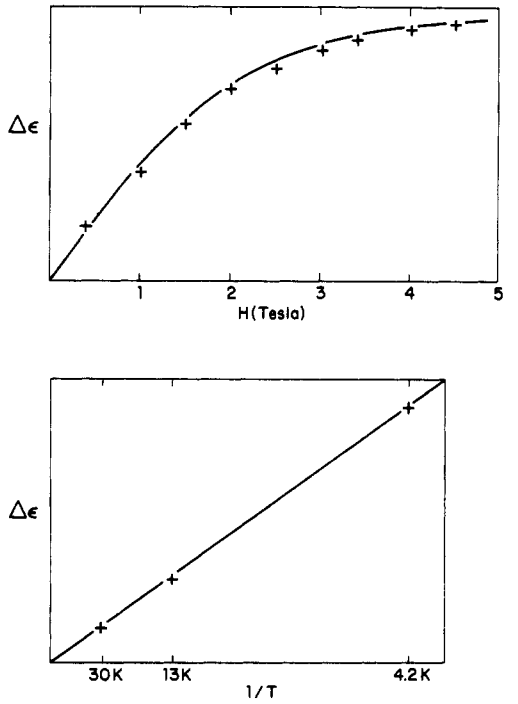

Figure 2. Experimental (+) and theoretical (solid curve) saturation behavior (upper panel) and temperature dependence (lower panel) of $FeCl_6^{3-}$ doped into Cs_2NaYCl_6. $\Delta\epsilon$ is the MCD in arbitrary units monitored at any frequency for which $\Delta\epsilon \neq 0$. The upper solid curve is eq 8, and the lower solid curve is a straight line through the origin.

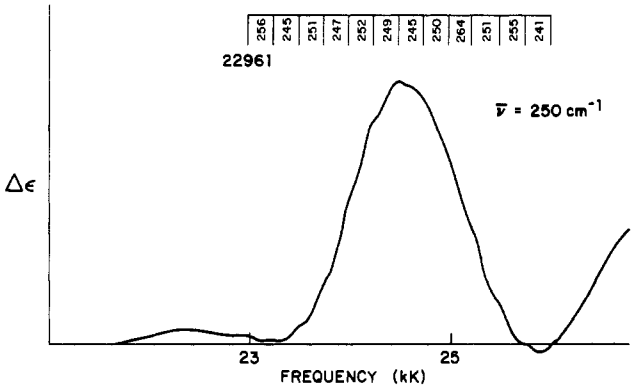

Figure 3. Vibrational progression observed in the MCD of band 2 starting at 22961 cm^{-1}.

The MCD saturation behavior is not a simple tanh form[25] since the ground state splits into six equally spaced sublevels in the magnetic field. However, the Zeeman pattern is isotropic and hence an explicit expression for the MCD temperature dependence may be derived. Evaluating eq 9–11 of ref 25 for $^6A_{1g} \rightarrow {}^6T_{1u}$, we obtain

$$\Delta\epsilon = \frac{K[(-e^{-G/2} + e^{G/2}) + (-e^{-3G/2} + e^{3G/2}) + (-e^{-5G/2} + e^{5G/2})]}{e^{-G/2} + e^{G/2} + e^{-3G/2} + e^{3G/2} + e^{-5G/2} + e^{5G/2}} \quad (8)$$

where $\Delta\epsilon$ is the MCD at an arbitrary frequency in the region of interest, $G \equiv g\mu_B H/kT$, and K is a proportionality constant, which is evaluated by fitting $\Delta\epsilon$ vs. H in the linear region (whence $e^{\pm G} \approx 1 \pm G$). A plot of eq 8 for the case $g = 2.0$ is shown by the solid curve in Figure 2 (upper panel), and the experimental points are shown by +'s. The fit is good and confirms that the optical spectrum is for a $g \approx 2$ species,

(25) Schatz, P. N.; Mowery, R. L.; Krausz, E. R. *Mol. Phys.* **1978**, *35*, 1537.

consistent with the ESR result[18] mentioned earlier.

Figure 3 shows a vibrational progression on the first prominent MCD band which is not apparent in absorption. The interval is 250 ± 6 cm^{-1}, which we assign to the totally symmetric Fe–Cl stretch in the first $^6T_{1u}$ excited state. The corresponding ground-state frequency is 285 cm^{-1}.[26] The observed 12% reduction corresponding to the ligand-to-metal electron transfer seems quite reasonable.

Seven transitions with ϵ_{max} values ranging from ~73 to 1740 can be identified in the absorption spectrum between 20 000 and 46 000 cm^{-1}. The lowest energy weak absorption at ~ 22 4000 cm^{-1} is assigned to the parity-forbidden ligand-to-metal excitation, $t_{1g} \rightarrow t_{2g}$. This excitation characteristically produces the lowest charge-transfer transition observed in the octahedral transition-metal hexahalides.[1,3,5-8] The subsequent transitions are much more intense, and we discuss their assignment to dipole-allowed ligand-to-metal charge-transfer transitions.

Referring to Table II, we note that the energy intervals between bands 2 and 4 (7100 cm^{-1}), bands 3 and 5 (7100 cm^{-1}), and bands 6 and 7 (6700 cm^{-1}) are very similar. We suggest that this spacing corresponds to the energy difference between a given $t_{xu} \rightarrow t_{2g}$ transition and the corresponding $t_{xu} \rightarrow e_g$ transition. This energy difference may be estimated[27] as $10Dq - D$; D is a spin-pairing energy parameter given by $D = {}^7/_6(5B/2 + C)$, where B and C are Racah parameters.[27] From d → d absorptions in a diffuse powder reflectance spectrum, Dq and B ($=C/4$) for $FeCl_6^{3-}$ were respectively estimated as 1100 and 605 cm^{-1}.[11] Thus $10Dq - D \approx 6400$ cm^{-1}, consistent with our interpretation of the band 2–4, 3–5, 6–7 intervals. Furthermore, this interpretation in turn requires that the band 2–3 separation correspond to the spacing between the ligand $t_{1u}(\pi + \sigma)$ and ligand t_{2u} orbitals. The observed band 2–3 separation of 3000 cm^{-1} (Table II) is indeed typical of the $t_{1u}(\pi + \sigma)$–t_{2u} interval in other transition-metal hexahalides.[1,3,5-8]

Let us now compare the experimental MCD spectrum with the theoretical model. In view of our previous discussion, band 2 must correspond either to $t_{1u}(\pi + \sigma) \rightarrow t_{2g}$ or $t_{2u} \rightarrow t_{2g}$. Using parameters that are discussed in detail later, we show MCD stick patterns in Figure 4 calculated using both the simple (dotted sticks) and full (solid sticks) treatment of spin–orbit coupling. (No reasonable variation of parameters wil change the qualitative nature of these patterns). Examining Figure 4 (for the full treatment), we note for $t_{1u}(\pi + \sigma) \rightarrow t_{2g}$ that the single most intense MCD feature is predicted to be positive and should be located ~100 cm^{-1} to the red of the absorption maximum. This contrasts with the case for $t_{2u} \rightarrow t_{2g}$ (Figure 4), where the most intense MCD feature is predicted to be negative with a location about 300 cm^{-1} to the blue of the absorption maximum. In fact the observed MCD shows a large (positive) maximum about 300 cm^{-1} to the red of the band 2 absorption peak and a large (negative) minimum about 300 cm^{-1} to the blue of the band 3 absorption peak. It is thus very plausible to associate bands 2 and 3, respectively, with the excitations $t_{1u}(\pi + \sigma) \rightarrow t_{2g}$ and $t_{2u} \rightarrow t_{2g}$. (Then the predicted negative, higher energy MCD of $t_{1u}(\pi + \sigma) \rightarrow t_{2g}$ is largely canceled by the positive MCD of the low-energy region of $t_{2u} \rightarrow t_{2g}$.) This ordering is conclusively confirmed by the MCD of band 4 in view of our earlier discussion. Thus if band 2 goes with $t_{1u}(\pi + \sigma) \rightarrow t_{2g}$, band 4 must be associated with $t_{1u}(\pi + \sigma) \rightarrow e_g$. The observed MCD pattern of band 4 agrees with the predicted pattern for this excitation (Figure 4) and is opposite to the predicted pattern for $t_{2u} \rightarrow e_g$. The latter excitation would be associated with band 4 if the assignments of bands 2 and 3 were interchanged. Therefore, the energy ordering of the ligand orbitals is $t_{1g} > t_{1u}(\pi + \sigma) > t_{2u} > t_{1u}(\sigma + \pi)$, as has been previously observed in all the other transition-metal hexahalides.[1,3,5-8]

Let us now consider the theoretical MCD band simulation. This was synthesized in several steps. First, the reduced transition moment matrix element, $|\langle {}^6A_{1g} \| m \| {}^6T_{1u} \rangle|$, was empirically established for each of bands 2–4 by choosing values via eq 5 that reproduced the experimental dipole strengths (eq 7). (These matrix elements are required when we subsequently calculate $\mathcal{C}_0$ for each transition via eq 4.) The line width (Δ_i, eq 6) was then assigned a fixed value for all transitions in a given band (i.e., for all transitions within a given excitation $t_{xu} \rightarrow t_{2g}$ or e_g) such that it reasonably reproduced the observed absorption band width. The resonance frequencies ($\nu_0(i)$, eq 6) for bands 2–4 were simultaneously chosen to reproduce the experimental absorption band positions. (The resulting fit of the absorption spectrum is shown by the dashed curve in Figure 1.)

With these parameters chosen, it is now possible to synthesize the MCD pattern for bands 2–4 by carrying out the diagonalization of the spin–orbit coupling matrix within each $^{2S_4+1}\Gamma_4$ manifold in Table I, as discussed previously in part B of the Theory section. This diagonalization depends upon three parameters, namely, ζ_{Fe}, ζ_{Cl}, and the σ–π mixing parameters (a or b) defined by

$$\begin{aligned} t_{1u}(\pi + \sigma) &= a(t_{1u}(\sigma)) + b(t_{1u}(\pi)) \\ t_{1u}(\sigma + \pi) &= -b(t_{1u}(\sigma)) + a(t_{1u}(\pi)) \\ a > 0 \qquad b > a \qquad a^2 + b^2 &= 1 \end{aligned} \tag{9}$$

In eq 9, the signs of a and b are chosen so that $t_{1u}(\pi + \sigma)$ is the higher energy, antibonding MO, and $t_{1u}(\sigma)$ and $t_{1u}(\pi)$ are defined in Table III. Since the t_{1u} and t_{2u} orbitals are ligand centered, the orbital angular momentum operator is expanded in terms of ligand-centered operators[4,14,22] to permit evaluation of matrix elements of the form $\langle A\alpha|L_Z|A\alpha \rangle$ in eq 4. The resulting reduced matrix elements are listed in Table IV.

A "best fit" of the observed MCD spectrum of bands 2–4 was obtained by systematically varying ζ_{Fe}, ζ_{Cl}, and a (or b). The results for the full treatment are shown by the dashed curve in Figure 5 for the parameters $\zeta_{Fe} = 320$ cm^{-1}, $\zeta_{Cl} = 580$ cm^{-1}, and $b = 0.95$. For bands 5–7, it was not possible to fix precise values for $\langle {}^6A_{1g} \| m \| {}^6T_{1u} \rangle$, Δ_i and $\nu_0(i)$ by fitting the

Table III.[a,b] $t_{1u}x$ and $t_{2u}\xi$ Components of Ligand Orbitals[c]

	σ	π
$t_{1u}x$	$-(1/2^{1/2})(p_{x_1} + p_{x_3})$	$-{}^1/_2(p_{x_2} + p_{x_4} + p_{x_5} + p_{x_6})$
$t_{2u}\xi$		$-(i/2)(p_{y_5} - p_{y_6} + p_{z_2} - p_{z_4})$

[a] The coordinate system is from ref 3; all atoms have parallel right-handed systems and the chlorides are numbered: 1 $(R, 0, 0)$, 2 $(0, R, 0)$, 3 $(-R, 0, 0)$, 4 $(0, -R, 0)$, 5 $(0, 0, -R)$, 6 $(0, 0, R)$. [b] The relation of the present basis functions[22] (written here as kets) to the Griffith basis[28] written here without the ket notation is as follows: $|t_1x\rangle = -x$, $|t_1y\rangle = iy$, $|t_1z\rangle = z$; $|t_2\xi\rangle = -\xi$, $|t_2\eta\rangle = -i\eta$, $|t_2\zeta\rangle = \zeta$. [c] Phases of $t_{1u}y$, $t_{1u}z$, $t_{2u}\eta$, and $t_{2u}\zeta$ were chosen such that standard basis relations of the group chain $O \supset D_4 \supset D_2 \supset C_2$ ("real" O basis)[22] are satisfied.[21]

Table IV. Reduced One-Electron Orbital Angular Momentum Matrix Elements[a]

reduced matrix element	value
$\langle t_{2g} \| \xi l^{t_1u} \| t_{2g} \rangle$	$-6^{1/2}\zeta_{Fe}$
$\langle t_{1u}(\pi + \sigma) \| \xi l^{t_1u} \| t_{1u}(\pi + \sigma) \rangle$	$-6^{1/2}\zeta_{Cl}[(b^2/2) + 2^{1/2}ab]$
$\langle t_{1u}(\sigma + \pi) \| \xi l^{t_1u} \| t_{1u}(\sigma + \pi) \rangle$	$-6^{1/2}\zeta_{Cl}[(a^2/2) - 2^{1/2}ab]$
$\langle t_{2u} \| \xi l^{t_1u} \| t_{2u} \rangle$	$-(6^{1/2}/2)\zeta_{Cl}$

[a] ζ_{Fe} and ζ_{Cl} are the one-electron spin–orbit coupling constants, and a and b are the π–σ mixing parameters defined in eq 9. Butler's phase definitions are used[21]—see footnote *b*, Table III.

(26) Nakagawa, I. *Can. J. Spectrosc.* **1973**, *18*, 1.
(27) Jørgensen, C. K. "Orbitals in Atoms and Molecules"; Academic Press: New York, 1962; p 22.

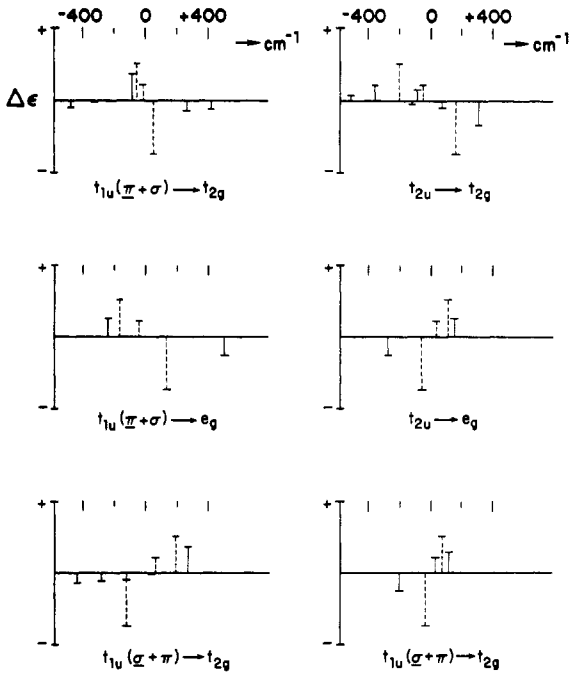

Figure 4. Theoretical $\mathcal{C}$-term stick patterns of each excitation for the full (solid bars) and simple (dashed bars) treatments using the respective parameters $\zeta_{Fe} = 320$ cm^{-1}, $\zeta_{Cl} = 580$ cm^{-1}, $b = 0.95$ and $\zeta_{Fe} = 120$ cm^{-1}, $\zeta_{Cl} = 580$ cm^{-1}, $b = 0.98$. The height of each stick is directly proportional to $\mathcal{C}_0^{(i)}$ (eq 2). The zero of energy is the absorption band maximum, and the vertical scales ($\Delta\epsilon$) are arbitrary. The sum of stick heights (solid or dashed) for each excitation is zero because the ground state is orbitally nondegenerate.

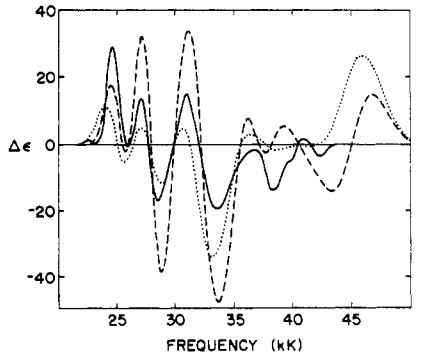

Figure 5. Experimental MCD (solid curve) and theoretical simulations using the full treatment (dashed curve) with $\zeta_{Fe} = 320$ cm^{-1}, $\zeta_{Cl} = 580$ cm^{-1}, and $b = 0.95$ and simple treatment (dotted curve) with $\zeta_{Fe} = 120$ cm^{-1}. $\zeta_{Cl} = 580$ cm^{-1}, and $b = 0.98$. The $\nu_0(i)$, Δ_i, and $\mathcal{D}_0^{(i)}$ values used are given in the caption for Figure 1.

absorption spectrum in view of the poor definition and rising absorption edge of the crystal host. So $\nu_0(i)$ values were estimated from the apparent peak locations and $\langle {}^6A_{1g}||m||{}^6T_{1u}\rangle$ and Δ_i were simply chosen for bands 5 and 6 to give magnitudes and widths consistent with the experimental absorption and MCD, which in fact has only qualitative significance beyond about 38 000 cm^{-1}. The estimates of $\langle {}^6A_{1g}||m||{}^6T_{1u}\rangle$ and Δ_i for band 7, whose MCD is out of range, are quite arbitrary.

A "best fit" of the MCD is also shown by the dotted curve in Figure 5 for the simple treatment (where spin–orbit splitting only *within* each ${}^6T_{1u}$ state is considered). The parameters obtained were $\zeta_{Fe} = 120$ cm^{-1}, $\zeta_{Cl} = 580$ cm^{-1}, and $b = 0.98$.

Discussion

While both the "full" and "simple" treatments of spin–orbit coupling give semiquantitative agreement with the experimental MCD, only the former is able to do so with physically reasonable parameters. In particular the simple treatment requires $\zeta_{Fe} \approx 120$ cm^{-1}, a value that is far too small in view of the estimated free ion value of 410 cm^{-1} (ref 28, Appendix 6). Fits attempted with more realistic (higher) values of ζ_{Fe} significantly increase the discrepancy between the theoretical and experimental MCD patterns. The value $\zeta_{Fe} = 320$ cm^{-1} found in the full treatment is about 20% lower than the free ion value, a very resonable reduction for a hexahalide system. $\zeta_{Cl} = 580$ cm^{-1} is very close to the value widely used in the literature (587 cm^{-1}). Note also that the full treatment gives a distinctly better fit of the band 2 MCD pattern.

The small σ–π mixing implied by our fit ($b = 0.95$) is consistent with the roughly equal intensities observed for $t_{1u}(\pi + \sigma) \rightarrow t_{2g}$ and $t_{2u} \rightarrow t_{2g}$ since simple qualitative arguments[29] suggest equal intensity for $t_{1u}(\pi) \rightarrow t_{2g}$ and $t_{2u} \rightarrow t_{2g}$ (and zero intensity for $t_{1u}(\sigma) \rightarrow t_{2g}$).

We stress that our theoretical MCD simulation, particularly in the band 3–4 region, could be substantially improved by relatively minor adjustments. For example, because the calculated MCD pattern is a composite involving strong cancellations of nearby $\mathcal{C}$ terms of opposite sign (Figure 4), judicious adjustments of transition energies by a few tens of cm^{-1} would bring the theoretical MCD amplitudes into much better quantitative agreement with experiment. Clearly, our much simplified model can easily encompass energy shifts of this magnitude, and we would anticipate significantly improved agreement if electrostatic interactions between metal and ligand electrons could be reasonably treated. Neglect of spin–orbit interactions betweeen different ligand-to-metal excitations is probably a much less serious source of error.

Conclusions

The MCD spectrum of $FeCl_6^{3-}$ in the 20 000–45 000-cm^{-1} region can be explained semiquantitatively by using a simple model and assuming all spectral features arise from ligand-to-metal charge-transfer excitations. The model neglects interelectronic repulsions between ligand and metal electrons. To obtain reasonable parameters, it is essential to include spin–orbit interactions between each ${}^6T_{1u}$ excited state and the other sextet and quartet states that arise from the quintet Fe^{2+} state (and that by the model are accidentally degenerate with ${}^6T_{1u}$). The ordering of the ligand orbitals is the one universally observed in the transition-metal hexahalides: $t_{1g} > t_{1u}(\pi + \sigma) > t_{2u} > t_{1u}(\sigma + \pi)$. The spin–orbit coupling parameters that best fit the MCD are $\zeta_{Fe} = 320$ cm^{-1} and $\zeta_{Cl} = 580$ cm^{-1}. σ–π mixing in the t_{1u} ligand orbitals is small, $\sim$10%.

Acknowledgment. This work was supported by the Swiss National Science Foundation under Grant No. 2.427-0.79 and by the National Science Foundation under Grant No. CHE8025608. We are much indebted to Dr. Susan B. Piepho for her detailed guidance in the use of the chain of groups method for calculating spin–orbit matrix elements (see also the Appendix). K.N. acknowledges support under a Swiss NSF fellowship for the time period in Charlottesville.

Appendix. Calculation of Excited-State Spin–Orbit Coupling Matrix Elements

Method of Piepho[22] Using the Butler Chain of Groups Approach.[21] The basic formula is

$$\langle (ec)(\mathcal{S}S,h)tr\tau|\hat{\mathcal{H}}_{so}|(ec)'(\mathcal{S}'S',h')t'r'\tau'\rangle = -\delta_{tt'}\delta_{\tau\tau'}\{Shtr\}\{hT_1h'0\}\times$$
$$\left[\sum_y \begin{Bmatrix} S' & h' & t' \\ h & S & T_1 \end{Bmatrix}_{yor\tau'} \begin{pmatrix} \mathcal{S} & 1 & \mathcal{S}' \\ S & T_1 & S' \end{pmatrix}_{yO}^{SO_3}\right] \sum_k \langle (ec)\mathcal{S}h||\Sigma s^1 u^{t_1}(k)||(ec)'\mathcal{S}'h'\rangle \quad (10)$$

(28) Griffith, J. S. "The Theory of Transition-Metal Ions"; Cambridge University Press: New York, 1964.
(29) Jørgensen, C. K. "Absorption Spectra and Chemical Bonding in Complexes"; Pergamon Press: Oxford, England, 1962.

where (ec) designates electron configuration, $\mathcal{S}$ and S are total spin classified respectively in the irreducible representations (irreps) of groups SO_3 and O, h is the orbital irrep in group O, t is the resulting spinor irrep of $S\otimes h$ in group O, τ is the irrep component of t, and r is the multiplicity index used when $S\otimes h$ contains a repeated irrep. $\{Shtr\}$ is a $3-j$ phase factor

$$\begin{Bmatrix} S' & h' & t' \\ h & S & T_1 \end{Bmatrix}_{\gamma o r r'}$$

is a $6-j$ symbol, and

$$\begin{pmatrix} \mathcal{S} & 1 & \mathcal{S}' \\ S & T_1 & S' \end{pmatrix}^{SO_3}_{\gamma O}$$

is a $SO_3 \supset O$ chain $3jm$ factor. These latter three sets of quantities are tabulated by Butler.[21] The last quantity on the right-hand side of eq 10 is the many-electron reduced spin–orbit matrix element.

Let us consider an example. Suppose we wish to evaluate

$$\langle ({}^3/_2U',E)U'0\kappa|\hat{\mathcal{H}}_{so}|({}^5/_2U',T_1)U'1\kappa\rangle \qquad (11)$$

Then the factors on the right-hand side of eq 10 are as follows: $\{U'EU'0\} = -1$ and $\{ET_1T_10\} = +1$ (from table: O and T_d $3-j$ phases (p 439[21]))

$$\begin{Bmatrix} U' & T_1 & U' \\ E & U' & T_1 \end{Bmatrix}_{0001} = 1/(2\sqrt{6})$$

$$\begin{Bmatrix} U' & T_1 & U' \\ E & U' & T_1 \end{Bmatrix}_{1001} = 0$$

(from Table: O and T_d $6-j$ symbols (p 440[21]) after application of eq 3.3.18 and 3.3.19 (p 59[21]))

$$\begin{pmatrix} {}^3/_2 & 1 & {}^5/_2 \\ U' & T_1 & U' \end{pmatrix}^{SO_3}_{0O} = 2\sqrt{2}/\sqrt{15}$$

$$\begin{pmatrix} {}^3/_2 & 1 & {}^5/_2 \\ U' & T_1 & U' \end{pmatrix}^{SO_3}_{1O} = -\sqrt{2}/\sqrt{15}$$

(from table: SO_3–O $3jm$ factors (p 262[21])). Then with use of eq 10, the right-hand side of eq 11 becomes

$$(-1)(-1)(+1)\left[\frac{1}{2\sqrt{6}}\frac{2\sqrt{2}}{\sqrt{15}} - 0\,\frac{\sqrt{2}}{\sqrt{15}}\right]\times \left\langle \tfrac{3}{2}E\|\sum_k s^1u^{t_1}(k)\|\tfrac{5}{2}T_1\right\rangle = \frac{1}{3\sqrt{5}}\left\langle \tfrac{3}{2}E\|\sum_k s^1u^{t_1}(k)\|\tfrac{5}{2}T_1\right\rangle \qquad (12)$$

Method of Griffith.[19,20] The Griffith formula analogous to eq 10 is eq 9.30:[19]

$$\langle \mathcal{S}hJt\tau|\hat{\mathcal{H}}_{so}|\mathcal{S}'h'J't'\tau'\rangle = \Omega_{JJ'}\begin{pmatrix} \mathcal{S} & \mathcal{S}' & T_1 \\ h' & h & t \end{pmatrix}\langle \mathcal{S}h\|\sum_k su(k)\|\mathcal{S}'h'\rangle \qquad (13)$$

where $\mathcal{S}$, h, t, and τ have the same significance as in eq 10, J is a pseudo angular momentum quantum number defined in §9.6.3,[28] and

$$\Omega_{JJ'}\begin{pmatrix} \mathcal{S} & \mathcal{S}' & T_1 \\ h' & h & t \end{pmatrix} = \sum_{iMM'\theta\theta'}(-1)^{1+\mathcal{S}-M'}[-1]^{h+\theta}\bar{V}\begin{pmatrix} \mathcal{S} & \mathcal{S}' & 1 \\ -M & M' & i \end{pmatrix}\times V\begin{pmatrix} h & h' & T_1 \\ -\theta & \theta' & -i \end{pmatrix}\langle \mathcal{S}hJt\tau|\mathcal{S}hM\theta\rangle\langle \mathcal{S}'h'M'\theta'|\mathcal{S}'h'J't\tau\rangle \qquad (14)$$

where the $\bar{V}$ values are available in Rotenberg et al.[30] and the V values are available in Griffith (Table C2.3, p 111[19]). The crucial difference here from the Piepho–Butler method is that the coupling coefficients (the two brackets on the right-hand side of eq 14) require the construction of wave functions. Let us illustrate by an example analogous to eq 11, which in Griffith notation reads

$$\left\langle {}^4\mathrm{E}\ U'\kappa|\hat{\mathcal{H}}_{so}|{}^6\mathrm{T}_1\ \frac{7}{2}U'\kappa\right\rangle \qquad (15)$$

Then according to the methods of §9.6.3[28] and Table A.20[28]

$$|{}^4\mathrm{E}\ U'\kappa\rangle = \frac{1}{\sqrt{2}}|{}^4\mathrm{E}\ \frac{3}{2}\theta\rangle + \frac{1}{\sqrt{2}}|{}^4\mathrm{E} - \frac{1}{2}\epsilon\rangle \qquad (16)$$

and with use of Table A.19[28]

$$|{}^6\mathrm{T}_1\ \frac{7}{2}U'\kappa\rangle = \frac{1}{2}|{}^6\mathrm{T}_1\ \frac{7}{2}-\frac{5}{2}\rangle + \frac{\sqrt{3}}{2}|{}^6\mathrm{T}_1\ \frac{7}{2}\frac{3}{2}\rangle \qquad (17)$$

where the kets on the right are in the $|^{2\mathcal{S}+1}h\ JM_J\rangle$ basis. Transforming eq 17 to the SO_3 basis (where the kets are $|^{2\mathcal{S}+1}h\ M_s\theta\rangle$) using appropriate Clebsch–Gordan coefficients[30] gives

$$|{}^6\mathrm{T}_1\ \frac{7}{2}U'\kappa\rangle = \frac{\sqrt{3}}{\sqrt{84}}|{}^6\mathrm{T}_1\ \frac{5}{2}-1\rangle + \frac{\sqrt{30}}{\sqrt{84}}|{}^6\mathrm{T}_1\ \frac{3}{2}0\rangle + \frac{\sqrt{30}}{\sqrt{84}}|{}^6\mathrm{T}_1\ \frac{1}{2}1\rangle + \frac{\sqrt{15}}{\sqrt{84}}|{}^6\mathrm{T}_1\ -\frac{3}{2}-1\rangle + \frac{\sqrt{6}}{\sqrt{84}}|{}^6\mathrm{T}_1\ -\frac{5}{2}0\rangle \qquad (18)$$

Then finally from eq 14

$$\Omega_{(3/2)(7/2)} = \frac{1}{\sqrt{6}}\frac{1}{2\sqrt{3}}\frac{1}{\sqrt{2}}\frac{\sqrt{3}}{\sqrt{84}} + \frac{1}{\sqrt{15}}\frac{1}{\sqrt{3}}\frac{1}{\sqrt{2}}\frac{\sqrt{30}}{\sqrt{84}} + \frac{1}{2\sqrt{15}}\frac{1}{2\sqrt{3}}\frac{1}{\sqrt{2}}\frac{\sqrt{30}}{\sqrt{84}} + \frac{1}{2\sqrt{5}}\frac{1}{2}\frac{1}{\sqrt{2}}\frac{\sqrt{30}}{\sqrt{84}} + \frac{1}{\sqrt{10}}\frac{1}{2}\frac{1}{\sqrt{2}}\frac{\sqrt{15}}{\sqrt{84}} \qquad (19)$$

where the phase factors and values of $\bar{V}$ and V have been explicitly inserted and the last two factors in each term are the coefficients from eq 16 and 18, respectively. In order to work out all of the required spin–orbit matrix elements in our treatment of the $FeCl_6^{3-}$ problem, a minimum of 31 wave functions of the form of eq 16 or eq 18 must be constructed. And if one wishes to make orthogonality or phase checks, additional functions are required. Furthermore, in the case of $^{2\mathcal{S}+1}T_2$ functions, if $\mathcal{S}\otimes T_2$ contains U' or E, an additional transformation is necessary (see §9.6.3[28]). Thus it should be clear that the Piepho–Butler method is much quicker and less prone to error. We note that the value of $\Omega_{(3/2)(7/2)}$ obtained from eq 19, viz., $1/(2(7^{1/2}))$, when inserted into eq 13 gives a result diferent from eq 12. This happens because $U'0$ and $U'1$ of Butler differ from $U'^3/_2$ and $U'^5/_2$ of Griffith by a similarity transformation.[21,22] When the full U' spin–orbit matrices are diagonalized, both methods will of course give the same eigenvalues.

The reduction of the many-electron reduced matrix elements (right-hand side of eq 12 or eq 13) is carried out in a similar way in both treatments; the details are given elsewhere.[19,20,22] Explicit application to a three-open-shell case has appeared in the literature.[12]

Finally, the transformation coefficients of the $|{}^6\mathrm{T}_{1u}M_s\theta\rangle$ functions required to calculate $\mathcal{C}_0$ and $\mathcal{D}_0$ (eq 4 and 5) are obtained from the $|{}^6\mathrm{T}_{1u}t\tau\tau\rangle$ functions by using eq 3.1.5 of Butler.[21]

Registry No. $FeCl_6^{3-}$, 19639-41-9.

(30) Rotenberg, M.; Bivins, R.; Metropolis, N.; Wooten, J. K. "The 3-j- and 6-j-symbols"; Technology Press, Massachusetts Institute of Technology: Boston, 1959.